Communication

Giant Enhancement of Photoluminescence Emission in WS2-2D Perovskite Heterostructures

Arky Qin Yang, Jean-Christophe Blancon, Wei Jiang, Hao Zhang, Joeson Wong, Ellen X. Yan, Yi Rung Lin, Jared J. Crochet, Mercouri G. Kanatzidis, Deep Jariwala, Tony Low, Aditye Mohite, and Harry A Atwater

Nano Lett., **Just Accepted Manuscript** • Publication Date (Web): 24 Jun 2019

Giant Enhancement of Photoluminescence Emission in WS_2-2D Perovskite Heterostructures

Arky Yang[1]*, Jean-Christophe Blancon[2]*, Wei Jiang[3], Hao Zhang[2], Joeson Wong[1], Ellen Yan[1], Yi-Rung Lin[1], Jared Crochet[2], Mercouri G. Kanatzidis[4], Deep Jariwala[1]**, Tony Low[3], Aditya D. Mohite[2]*** and Harry A. Atwater[1]***

*[1]California Institute of Technology, Pasadena, CA, 91125, USA. [2]Department of Chemical and Biomolecular Engineering, Rice University, Houston, TX 77005, USA. [3]Department of Electrical and Computer Engineering, University of Minnesota, Minneapolis, MN, 55455, USA. [4]Northwestern University, Evanston, IL, 60208, USA.*A. Yang and J. Blancon contributed equally to this work. **Currently at Department of Electrical and Systems Engineering, University of Pennsylvania, Philadelphia, PA 19104 USA.*

Keywords: Two dimensional materials; perovskite; transition metal dichalcogenide; heterostructure; interface; photoluminescence

Supporting Information Placeholder

ABSTRACT: Transition metal dichalcogenides (TMDCs) and two-dimensional organic and inorganic hybrid lead halide perovskites (2DPVSKs) have emerged as highly promising materials for ultralight and ultrathin optoelectronics application. They both exhibit tunability of electronic properties such as band structure, and they can form heterostructures with various types of two-dimensional materials for novel physical properties not observed in single components. However, TMDCs exhibit poor emission due to defect states and direct-to-indirect interband transition, and 2DPVSKs suffer from poor stability in ambient atmosphere. Here we report that fabrication of TMDC-on-2DPVSK heterostructures using a solvent-less process, leads to novel optical transitions unique to the heterostructure, which arise from the hybrid interface and exhibit a strong photoluminescence. Moreover a two orders of magnitude enhancement of the photoluminescence as compared to WS_2 emission is observed. The TMDC on top of 2DPVSK also significantly improves the stability as compared to bare 2DPVSK. Enhanced emission can be explained by electronic structure modification of TMDC by novel interfacial interactions between TMDC and 2DPVSK materials, which shows promise of the heterostructure for high efficiency and stable optoelectronic devices.

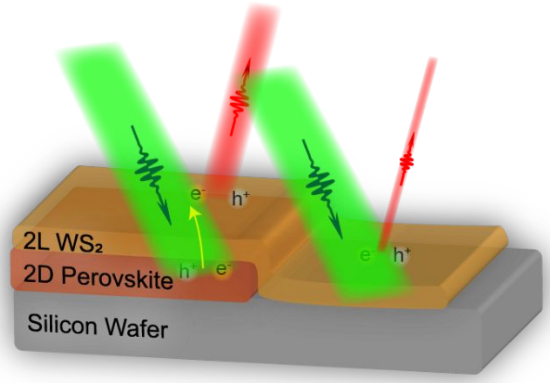

As two-dimensional (2D) semiconductors, transition metal dichalcogenides (TMDCs) have emerged as highly intriguing materials in the fields of optics[1,2], electronics[3,4], catalysis[5], and mechanics[6]. They also present some unique physical properties at the mono- and bi-layer level, such as valley polarization effects that allows controlling of spin carriers by light polarization, and led to development of the field of valleytronics in information processing. However, many optoelectronic applications of these materials are limited by their low photoluminescence quantum yield (PL QY), especially at multilayer thicknesses.[7,8]

Another family of 2D materials - organic-inorganic (hybrid) layered perovskite materials have also emerged as serious candidates for optoelectronic and information technologies. In contrast to TMDCs, layered perovskites not only present unique physics at the monolayer level but also preserve these properties in microscopic thin film devices, such as in solar cells[9,10] and light emitting diodes[11,12,13,14,15] (LEDs). Notably, hybrid 2D perovskites (2DPVSKs) are able to sustain large density of current[10] (>10 mA/cm^2) and yield reasonably high PLQY values of several to twenty percents[12,16,17]. However, 2DPVSKs are susceptible to ambient environmental[18] (oxygen, humidity, temperature, etc.) degradation as compared to purely inorganic materials, which has limited the exploration of their fundamental photo-physical properties.

Recent efforts have aimed at exploring their unique physical properties by creating hierarchical stacks of different 2D materials.[19,20] Here, we investigate the physical properties of a new type of vertical heterostructure composed of a few layers of TMDCs and 2DPVSKs. By creating an atomically-thin interface between these two types of materials, we were able to identify a two-order of magnitude enhancement in photoluminescence emission and improved air stability as compared to the TMDC and 2DPVSK, respectively. We also investigated the underlying mechanisms for the enhancement in heterostructure photoluminescence with a combination of time-resolved photoluminescence (TRPL) spectroscopy, ultra-violet photoemission spectroscopy (UPS), and materials

modeling, where plausible mechanisms for this enhancement is discussed. The giant enhancement of photoluminescence combined with relatively good air stability makes this heterostructure highly promising for ultrathin and ultralight optoelectronic devices. We believe that by creating a functional heterostructure platform combining inorganic and hybrid materials such as TMDCs and 2DPVSKs, this work presents a unique opportunity to quantitatively understand and tailor the interfacial coupling and electronic structure of such dissimilar hierarchical assemblies by tuning the chemical composition, structure and thickness of each of the materials under external stimuli such as light, electric field and strain. [15-26]

Figures 1a and 1b depict the layered structure of, respectively, the WS_2 TMDC and the Ruddlesden-Popper $BA_2MA_3Pb_4I_{13}$ hybrid 2D perovskite (abbreviated as either 2DPVSK or n=4 in the rest of the text) which are investigated here. The thickness of a single WS_2 and single perovskite layer are 0.315 nm and 2.51 nm, respectively. For both, strong carrier confinement effects in the layer plane, which is manifested by a strong anisotropy in optoelectronic and mechanical properties,[10,21] as well as unique photophysics[17,22] such as quantum confinement effects and large exciton binding energies[23,24]. The main difference in the structure of these two materials is that the WS_2 layers are electronically coupled across layers while the layers of perovskites are separated from one another by a thin (~0.7 nm) layer of organic materials (butylammonium BA) and maintains electronic properties of individual layers. The heterostructure (Fig.1c) was constructed by exfoliating 2DPVSK and dry viscoelastic stamping WS_2 on a silicon substrate (Si with a top 285 nm layer of SiO_2); these processes took place under inert atmosphere to prevent contamination of the interface and degradation of the 2DPVSK (Supplementary Fig. 1). The sample was identified under an optical microscope. Optical image of the sample demonstrates the presence of three regions– bare WS_2, bare n=4 2DPVSK, and heterostructure (Fig. 1d). From the image optical contrast and Raman spectroscopy (Fig. 1e) we conclude that the WS_2 flake is two layers thick and the n=4 2DPVSK about three layers thick[25]. The bare WS_2 flake yields Raman resonances at 351 and 418 cm^{-1}, corresponding to E^2_g and A^1_g vibration modes, respectively. The 67 cm^{-1} separation between the two WS_2 Raman peaks indicates that the WS_2 is double layer (2L).[7] The A^1_g mode is related to out-of-plane vibration of sulfur atoms and is sensitive to doping levels,[26,27] while the E^2_g mode is associated with the in-plane vibration of tungsten and sulfur atoms and is sensitive to strain.[28] The heterostructure presents the same Raman spectrum almost identical to the bare WS_2 flake within the resolution of our instrument (Fig. 1e). These data indicate that the doping level is not significantly altered to be observed in Raman spectra (i.e. a doping of more than $6*10^{12}/cm^2$ is needed to register a Raman shift surpassing the instrumental noise), and strain in the WS_2 layers in the heterostructure are unchanged as compared to the WS_2 by itself.[29] Based on our fabrication methods, the termination of the 2DPVSK at the interface can take one of several configurations: i) a single layer of BA molecules (the length of BA is about 0.6 nm) with half the density of that in a BA organic interlayer found in the 2DPVSK, ii) a layer of iodine atoms with a negative surface charge, which we can reasonably exclude from the lack of doping observed in the Raman data, or iii) a missing iodine atom in PbI_2 surface exposing a Pb^{2+} bond[30]. It is also reasonable to expect a non-homogeneous spatial distribution of the different types of termination enumerated above. The WS_2 is terminated with a layer of S atoms. Depending on the type of termination in the 2DPVSK, the WS_2/2DPVSK interface thickness could vary[31,32] and display a various degrees of hybridization between the WS_2 and 2DPVSK orbitals at their interface[30,33]. Although the lattice constant of the sulfur atom slab is about half the periodic arrangement of the organic BA molecules and perovskite octahedra (Fig. 1a,b), the Raman measurements does not indicate any appreciable strain in the WS_2. This is most likely due to the soft nature of the perovskite and organic layers, as well as the transfer process, which alleviates any significant strain at the interface[34,35].

Room temperature photoluminescence (PL) yield significant enhancement of the PL in the heterostructure as compared to

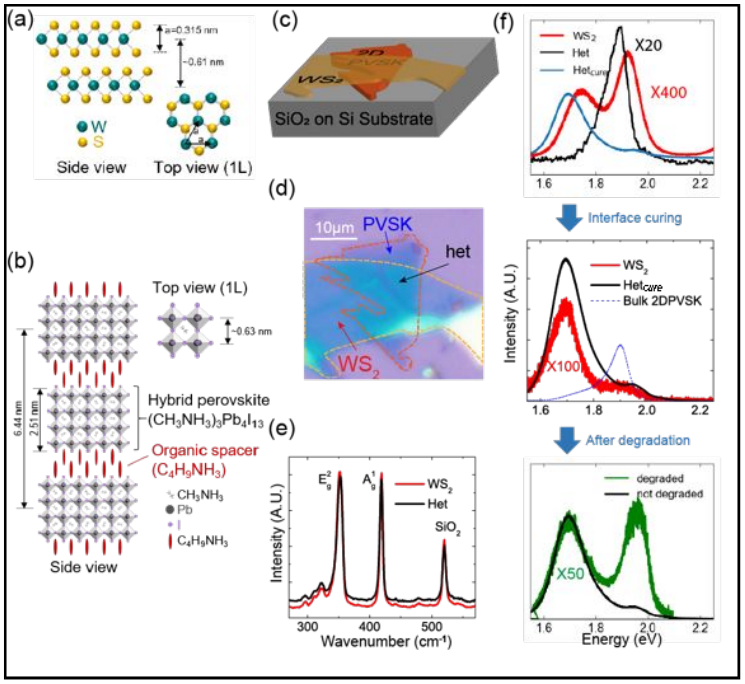

FIGURE 1. Crystal structures and lattice constants of WS_2 (a) and n=4 2DPVSK (b). (c) Schematic drawing of the heterostructure. (d) Optical image of the 2L WS_2 /n=4 2DPVSK heterostructure on SiO_2/Si substrate. (e) Raman spectra of the bare 2L WS_2 and the heterostructure taken in air at room temperature with 514 nm laser excitation. (f) PL spectra of the bare 2L WS_2, the n=4 2DPVSK and heterostructure, measured under ambient atmosphere with $3kW/cm^2$ at 514nm excitation.

the bare WS_2 and 2DPVSK (Fig. 1f). While at first the heterostructure shows a 20-fold enhancement in the PL integrated intensity as compared to the bare 2L WS_2, we found that after "interface curing" using laser annealing (with a 532 nm laser at a few kW/cm^2 in air for a few minutes) the PL enhancement reaches about 150 folds. After degradation of the sample the PL intensity decreases by more than 50 times. Before interface curing the heterostructure yields a single broad emission peak at about 1.9 eV. The bare WS_2 and the heterostructure after interface curing exhibit a broad peak at 1.69eV and a side feature at higher energy (Fig. 1f). The n=4 2DPVSK emits at around 1.9 eV with a low energy shoulder below 1.8 eV. The side feature in WS_2 is also around 1.9 eV, whereas the heterostructure side feature peaks at about 1.95 eV and the main peak in the heterostructure are broader than the bare WS_2. Again, the main difference between these samples is that the total PL of the heterostructure is enhanced up to 150 times as compared to the bare WS_2. We also note that center region of the heterostructure still showed strong emission even after 7 months of storage under nitrogen atmosphere and intermittent exposure to air, whereas luminescence emission from the bare 2DPVSK was not detectable due to sample degradation (Supplementary Fig. 2).[18,36] After degradation we observe a definite decrease in the PL intensity as shown in Fig. 1f. More significant decrease of intensity of lower energy peak comparing to the 1.9eV peak indicates that this degradation compromises interfacial interaction achieved through interface curing and is not reversible through further curing process. Our results indicate that WS_2 effectively encapsulates and stabilizes the 2DPVSK underneath it as discussed in the case of boron nitrite[18].

To show that this observation is not limited to the heterostructure in Fig. 1 we also investigated the 1L WS_2/ n=3 2DPVSK heterostructure (Supplementary Fig. 3). The 1L WS_2/ n=3 heterostructure yielded PL enhancements of about 25 times and 80 times before and after interface curing, respectively. It is important to note that after interface curing, the heterostructure PL spectrum is dominated by a broad feature at about 1.7 eV (Supplementary Fig. 3c), which is almost identical to the one observed for the 2L WS_2/n=4 heterostructure in Fig. 1f. Therefore, we infer that the PL feature at ~1.7 eV in the heterostructure of type WS_2/2DPVSK originates from states located at the heterostructure interface that are strongly activated via interface curing. These PL measurements demonstrate that combining WS_2 and 2DPVSK in an artificial heterostructure we have obtained materials with enhanced and more stable PL emission at room temperature.

In order to investigate the mechanism of PL enhancement and understand the features observed at room temperature we carried out measurements at low temperature (7K). Differential reflection spectra (defined as $(I_{sample}-I_{subrate})/I_{substrate}$, shown in Fig. 2a) exhibit absorption resonances corresponding to the A, B and C excitons for the bare WS_2, and the main exciton for the n=4 2DPVSK.[8,23] Additional peak between 1.85 and 1.95 eV emerging in the bare WS_2 were assigned to the defect states.[37] The bare n=4 2DPVSK exhibits absorption features around 1.95 eV, corresponding to exciton states and higher energy transitions as reported previously[23]. As illustrated in Fig. 2a, the reflection spectrum of the heterostructure is not the result of a simple sum of the component WS_2 and 2DPVSK layers, which is confirmed by the optical constants derived from the differential reflection data (Supplementary Fig. 4). Precisely, the lowest absorption resonance H_1 in the heterostructure is at the same energy (1.895 eV) as the perovskite exciton peak but with larger amplitude. On the other hand, resonances H_2 (1.945 eV) and H_3 (2.067 eV) are at about the same energy as the absorption peaks W_2 (also corresponding to n=4 exciton excited states) and A in WS_2 but with reduced amplitude. Similarly, higher energy transitions at 2.5eV and 2.7eV corresponding to n=4 features yield enhanced or similar absorption amplitude as compared to the bare n=4 2DPVSK. The B and C excitons in the 2L WS_2 are damped in the heterostructure (Supplementary Fig. 4). Additionally, we observe a strong resonance peak H_4 at 2.1 eV, which is not clearly present in either of the bare materials, except for a small feature in the bare 2DPVSK spectrum. This new feature was clearly measured using PL excitation (PLE) (Fig. 2b). All H4, H5, and H6 appear as strong absorption peak from the PLE data. The most notable observation from the PLE data is the 25-fold enhancement in the heterostructure as compared to the bare WS_2 and n=4 2DPVSK. Overall these results can be summarized as following: the heterostructure absorbs about 25 times more than n=4 2DPVSK and 2L WS_2. This is also accompanied (Supplementary Figure 4) by an overall decrease (resp. increase) of the refractive index as compared to the bare WS_2 (resp. n=4 2DPVSK).

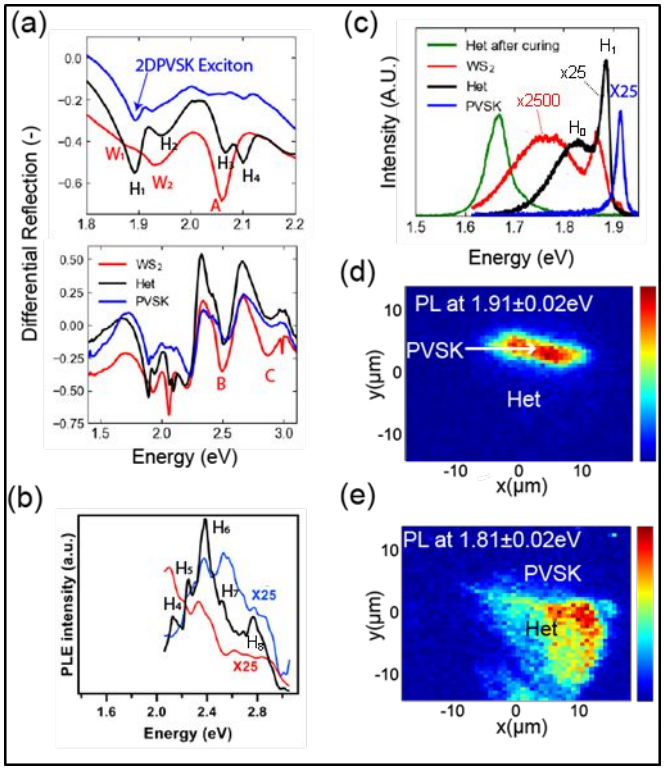

FIGURE 2. Optical properties at 7K of the 2L WS2/n=4 2DPVSK heterostructure compared to the bare WS_2 and n=4 2DPVSK. (a) Reflection spectra. (b) PL excitation spectra. (c) PL spectra, taken at 7K, at 550 nm laser excitation with intensity 5W/cm^2 for the bare n=4 and heterostructure, and 900 W/cm^2 for the 2L WS_2, and 100 W/cm^2 for heterostructure after curing. Intensities are scaled with power and integration time to show relative magnitude. (d) Map of n=4 2DPVSK exciton emission at 900W/cm^2 550 nm laser excitation with 5s integration per point.(e) Map of indirect emission of WS_2 at same condition. (color bar in intensity a.u.)

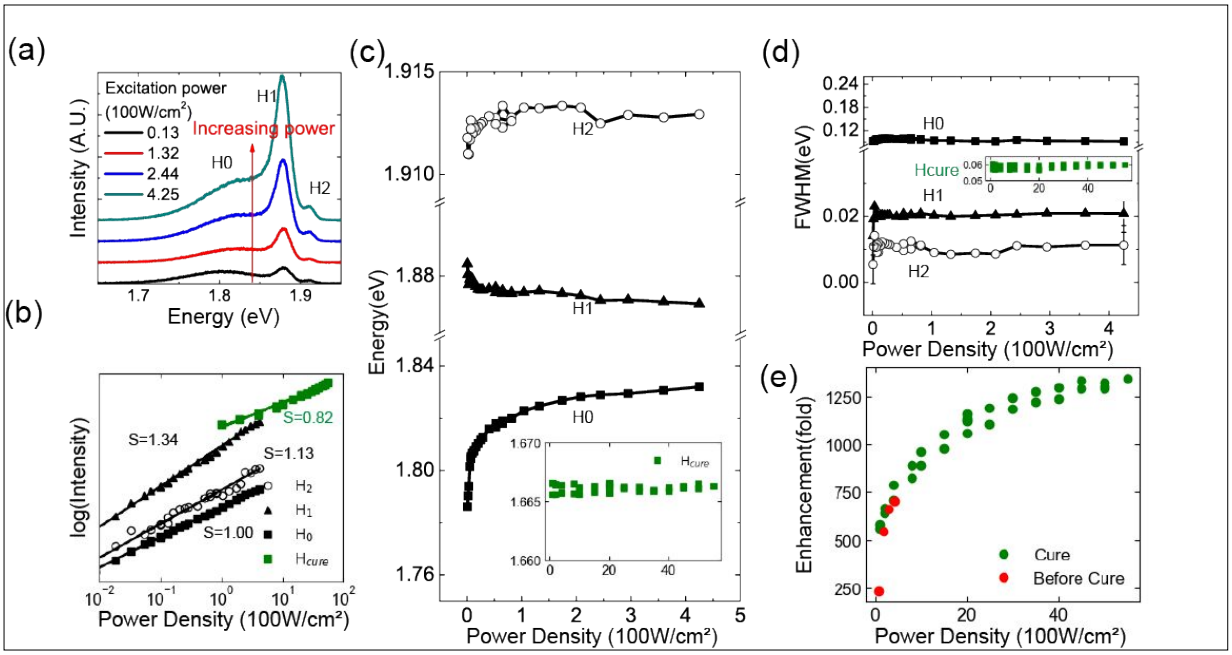

FIGURE 3. Power dependence of PL emission at 7K. (a) PL spectra of heterostructure taken at different incident laser power. Power dependence of (b) integrated PL intensity and (c) peak position of the PL transitions of the heterostructure. Green squares and line represent the data and fitted line after laser curing. (d) Corresponding power dependent of the FWHM. Inset: data of heterostructure after curing. (e) Enhancement of integrated PL intensity over all energy range measured on heterostructure verses bare WS_2.

In order to quantify the PL enhancement at low temperature and understand its origin, we analyzed the PL spectra at 7 K. The n=4 2DPVSK exhibits a single PL peak at 1.91eV with a Stokes shift of about 40 meV (Fig. 2c), which is identified as the exciton ground state.[23] The bilayer WS_2 PL spectrum yields two broad optical transitions: a broad emission at 1.75 eV with full width at half maximum (FWHM) 105meV, and a narrower emission line at 1.86eV (FWHM= 19meV). We also observed a small side feature at about 1.905 eV depending on the location on the sample (Supplementary Fig. 2). Based on previous reports[8,38,39], we attribute the broad emission around 1.75 eV due to defect state emission in bilayer WS_2. On the other hand, the heterostructure presents a relatively sharp PL peak at 1.87 eV (FWHM=16meV) with a broad shoulder around 1.83 eV, which are identified as H_1 and H_0, respectively. The main change in the heterostructure PL as compared to the individual constituent materials is a two orders of magnitude enhancement of the overall PL intensity as compared to the bare WS_2 with a similar emission spectrum (Fig. 2c). After interface curing the heterostructure PL spectrum is dominated by a broad PL peak at 1.65eV reminiscent of the 1.7 eV PL feature at room temperature. In this case, the heterostructure is enhanced by about three orders of magnitude as compared to the bare WS_2 and by 25-fold with respect to the bare n=4 2DPVSK before curing.

We performed the same study at low temperature on the 1L WS_2/n=3 2DPVSK. At 7 K, the monolayer WS_2 yields two emission features, one broad peak at 1.84eV and a narrow peak at 1.98eV (Supplementary Fig. 3d). These two peaks can be attributed to defect emission, since this emission disappears at room temperature in bare WS_2.[8] Here, we observe a 130-fold enhancement in the total PL of the heterostructure as compared to the bare 1L WS_2, a value on par with the heterostructure 2L WS_2/n=4 2DPVSK. The corresponding 50-fold enhancement in the heterostructure PL with respect to the bare n=3 2DPVSK is larger than in the 2L WS_2/n=4 2DPVSK heterostructure but could be explained by the beam damage on 2DPVSK due to prior measurements and different effective light intensity at the substrate surface due to interferences in the SiO_2. Reflection spectra (Supplementary Fig. 3e) show the presence of A and B exciton resonances of the monolayer WS_2 in both the WS_2 and the heteorstructure. The ground exciton state of the n=3 2DPVSK is observed at about 2.0 eV, at about the same energy as the W_1 feature of the 1L WS_2. Overall the reflection spectra leads to the conclusion that the absorption of the heterostructre is dominated by the 1L WS_2 in the low energy range (< 2.2 eV), and mainly shows 1L WS_2 features whereas the features of both the n=3 2DPVSK and 1L WS_2 (B exciton) are observed for energies larger than 2.2 eV. This is confirmed in the PLE spectra (Supplementary Fig. 3f). Similar to the 2L WS_2/ n=4 2DPVSK sample, the PLE spectum of the 1L WS_2/n=3 2DPVSK shows 250 times and 70 times higher PL in heterostructure compared to the bare n=3 PVSK and 1L WS_2 samples respectively.

Photoluminescence maps at peak emission energy for the n=4 2DPVSK and WS_2, are shown in Fig. 2d and Fig. 2e, respectively. At the n=4 2DPVSK exciton peak (1.91eV), strong emission of 2DPVSK is only observed in the bare 2DPVSK region, but not in the heterostructure. In contrast, strong defect state emission is observed in the heterostructure region only (1.81eV). These maps indicate that 2DPVSK emission is quenched under WS_2. Notice that the emission intensities also exhibit spatial variation over the sample, which can be attributed to spatially inhomogeneous layer thickness and coupling between layers (Supplementary Fig. 2).

More insights into the photophysics of the heterostructure were gained by investigating the power dependence of the PL spectra (Fig. 3, and Supplementary Fig. 5 for the 1L WS_2/n=3 heterostructure). The integrated PL of the two peaks H_0 and H_2 yields a close to linear dependence on the light excitation

intensity, whereas the main PL feature H_1 presents a super-linear intensity dependence with a coefficient of 1.35 (Fig. 3b). Additionally, we observe a ~40 meV blueshift of the energy of the PL peak H_0 with increasing excitation intensity (Fig. 3c) possibly due to state filling. On the other hand, the PL features H_1 undergoes a less than 5 meV redshift over the entire power range and for H_2 we observe a blueshift of less than 2 meV. We also observe no significant broadening of any of the PL features with excitation intensity (Fig. 3d). From these results, we conclude that the feature H_0 corresponds to defect bond exciton,[29] which undergoes energy band filling with excitation intensity. Similar to the WS_2 reflection spectra analysis, the main PL emission H_1 is identified as a biexciton state or mixed excitonic - free carrier states. It is confirmed by the super-linear power dependence of PL intensity.[29] We suggest this may be a signature of a partial dissociation of the exciton at the interface as reported previously for 2DPVSK edge surface or doping at the interface arising from the band alignment and bending. In that case, the redshift with increasing power could be the result of screening effects of the charge interactions at the interface where H_1 state can accumulate, concomitant with the saturation of the H_0 state. In contrast, heterostructure emission after interface curing exhibit slight sublinear power dependence of intensity (coefficient = 0.82), which could be a result of saturation of local states at interface with increasing power. Moreover, its peak position remains unshifted with changing power density, different from defect bound exciton state or indirect transition. This indicates that the PL emission from interface cured heterostructure has different origin than free excitons or band-to-band transition in 2L WS_2.

We observe a more than two order of magnitude increase in PL emission in the heterostructure as compared to the bare WS_2 over the applied range of excitation power density. Fig. 3e shows that this enhancement factor, corresponding the ratio between the integrated PL in the heterostructure and that in the bare WS_2, improves from about 220 at 0.8 kW/cm^2 to 700 at 4.4 kW/cm^2. This improvement is largely attributed to the enhancement of the H_1 state, shown in Fig. 3a.

To gain a deeper understanding of the PL enhancement in the heterostructures composed of TMDCs and 2DPVSK, we performed TRPL, UPS and transfer matrix calculations (TMM), Fig. 4 and Supplementary Fig. 6. TMM calculations indicate that the PL emission enhancement does not originate from an effect of dielectric environment change. Electric field and generation profiles were calculated for the heterostructure and the bare WS_2 at 550 nm (2.25 eV) and 660 nm (1.88 eV), corresponding to the laser excitation wavelength and for the main emission peak (Figure 4a and 4b). The generation rate per unit length for WS_2 in the heterostructure is higher than from the 2DPVSK in the heterostructure, but is nonetheless lower than that of bare WS_2, indicating the absence of a carrier generation enhancement in WS_2 layer. Calculated absorbance spectra (Fig.

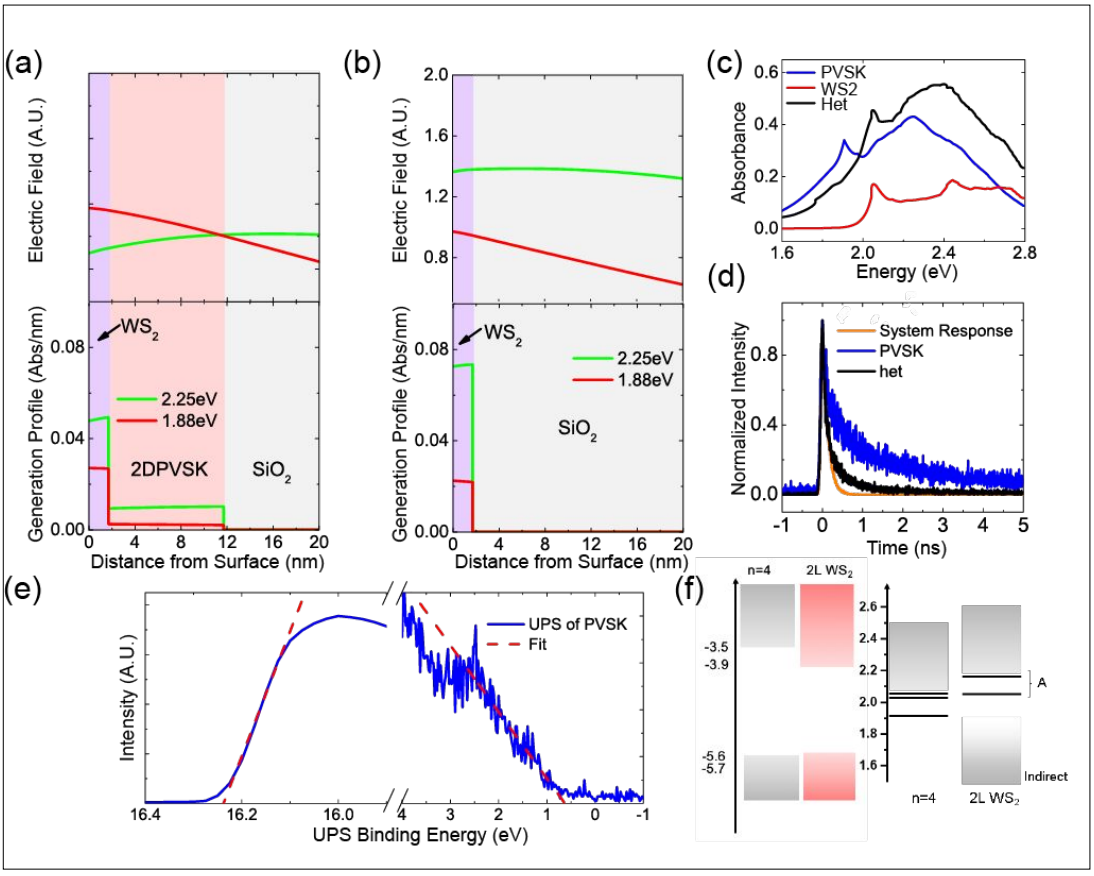

FIGURE 4. Transfer matrix calculation of heterostructure on 285nm SiO_2 on Si substrate. (a) Generation profile and electric field over depth of heterostructure at excitation emission wavelength in a full heterostructure and (b) WS2 only sample. (c) Calculated absorption spectra of three regions. (d) Time dependent photoluminescence spectra of heterostructure and n=4 2DPVSK taken at 2.25eV 4.25uW excitation and 1.88±0.2eV collection. (e) UPS spectra and fitting of n=4 2DPVSK. (f) Derived band positions of n=4 2DPVSK and 2L WS_2, with grey boxes indicating conduction and valance band forming direct band gap, and red box representing indirect band positions. (inset) Energy diagram in the excitonic picture for the bare n=4 2DPVSK and WS_2 samples taken from previous reports.[23,42,43] Black lines indicate the exciton Rydberg series.

4c) indicate that the absorbance of the heterostructure is larger than that of individual layers, but smaller than the sum of absorption from both materials confirming our results in Supplementary Fig. 4. Here, A, B, and 2DPVSK exciton peaks observed in reflection measurements (Fig. 2a) are consistent with absorption peaks calculated using transfer matrix method while H_4 cannot be explained. TMM calculation also shows 0.45 and 0.15 absorbance of WS_2 A exciton and H_3 peaks respectively, which is opposite to the reflectance spectra which shows larger dip in WS_2 A exciton, which is likely due to different level of transmission through these two regions and electronic effects. Since transfer matrix calculation do not show either an enhancement of WS_2 emission/absorption or a significant reduction of the n=4 2DPVSK emission/absorption in the heterostructure compared to the individual constituents, purely photonic effects, such as changes in the local dielectric environment, can be ruled out as the origin as the giant WS_2 PL enhancement. We also confirmed this observation by exfoliating 2L WS_2 on hexagonal Boron Nitride (hBN) and BA (Supplementary Figure 7). In both cases we observe little changes in the PL spectra and no significant photoluminescence enhancement. Figure 4e shows the UPS spectra and spectral fits at the high and low kinetic energy cut-off for the n=4 2DPVSK. The valence band energy for the 2DPVSK obtained from these cut-offs is -5.59eV referenced to the vacuum level. Literature values for the 2DPVSK band gap and band positions of WS_2[23,40,41,42], indicate that they form a Type I band alignment, with an energy level mismatch of about 472 meV and ~100 meV for the conduction band minimum and valence band maximum, respectively (Fig. 4f). We note that the energy difference of the conduction band minima between the 2L WS_2 and n=4 2DPVSK is of the order of the difference between the principle exciton energy in these materials and the 2L WS_2/n=4 heterostructure PL peak after interface curing. The relatively good energy correspondence between exciton states in both the 2L WS_2 and n=4 2DPVSK might promote dipole-dipole interactions as discussed in ref.[43].

TRPL (Fig 4d) measured for the bare 2DPVSK yields a lifetime slightly under the nanosecond time scale, in agreement with a previous report[17]. On the other hand, the reported lifetime of bilayer WS_2 is of the order of tens of picoseconds, attributed intervalley scattering[44]. The heterostructure exhibits an intermediate PL decay time between the bare WS_2 and n=4 2DPVSK indicative of either a charge transfer and/or dipole-dipole interactions mechanisms at the interface[43]. This can also be a consequence of the different nature of the photoemitting states at the interface.

The similarities in the results between the two heterostructures support a common mechanism for the origin of the photoluminescence enhancement in TMDCs/2DPVSK heterostructures. We hypothesize that a significant contribution to the PL enhancement in the heterostructures with respect to their bare constituents is due to their interface. Using first-principles calculation, we verified that the 2L WS_2/2DPVSK interface modifies electronic structure of 2L WS_2 and enables large PL enhancement. Microscopic insights about the heterostructures constructed by TMDCs and 2DPVSK have been obtained by first-principles calculation based on density functional theory (see Supporting information for calculation details). Heterostructures with different thickness of the 2DPVSK and WS_2 were systematically calculated. Figure 5(a) and (b) show the side and top view of the 2L WS_2/n=4 2DPVSK structures without the organic ligands, respectively. To understand the effect of the heterostructure interface, we first calculated the distribution of the charge transfer between 2L WS_2 and n=4 2DPVSK due to the heterostructure formation. As can be seen in Fig. 5(c), a clear charge transfer exists between WS_2 and 2DPVSK, where electrons (yellow) and holes (blue) are accumulated at the 2DPVSK and WS_2 side, respectively, and most of the transferred charges (electrons and holes) are distributed near the interface. Therefore, electrons are transferred from 2L WS_2 to 2DPVSK, resulting in the p-doping of the 2L WS_2. Such p-doping effect could compensate possible n-type doping in the as exfoliated WS_2 samples, leading to the enhancement of formation of exciton and thus the corresponding PL,[8] as observed in the experimental measurements.

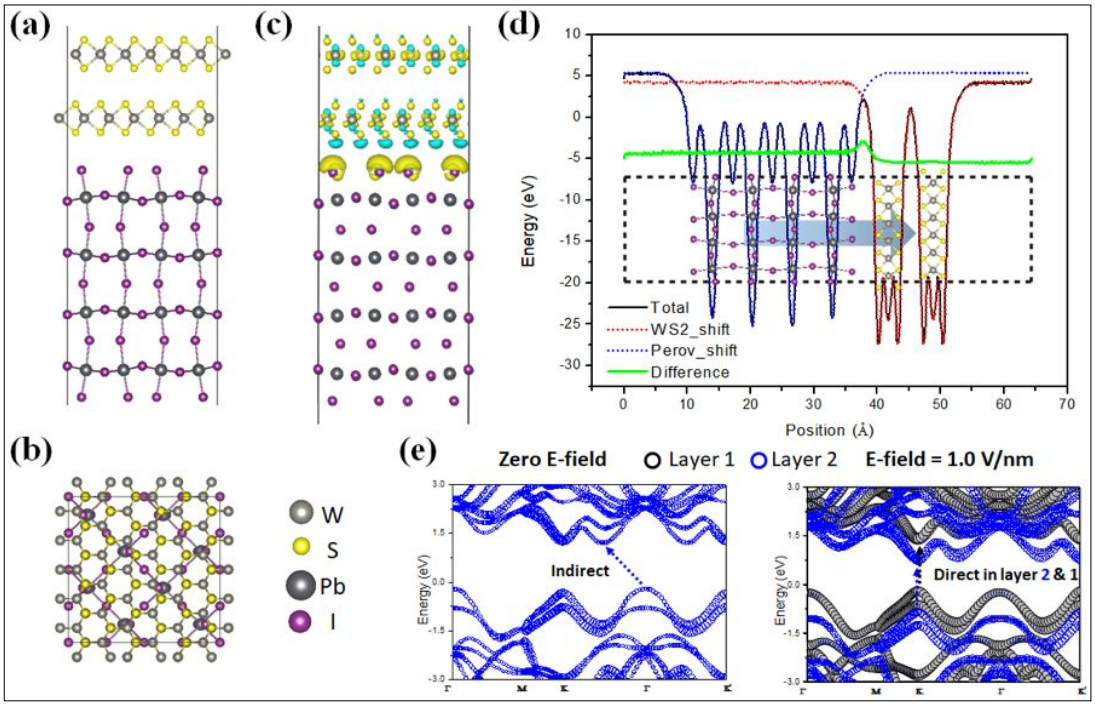

FIGURE 5. DFT calculations of heterostructure of 2L WS_2/n=4 2DPVSK. (a) and (b) Side and top view of the heterostructure, respectively. (c) Charge difference distribution of the heterostructure due to the formation of the interface. The yellow and blue color indicate the electrons and holes, respectively. (d) The plane-averaged potential profile of the heterostructure (black), WS_2 (red), 2DPVSK (blue), and the difference due to the formation of heterostructure (green), respectively. (e) The layer-resolved projected band structures (black and blue circles for two layers) of 2L freestanding WS_2 without and with E-field demonstrate the indirect to direct transition.

On the other hand, due to the charge transfer, an electronic dipole is formed across the heterostructure interface. As can be seen in Fig. 5(d), the difference of plane-averaged potential at the two sides of the heterostructure (black solid line) confirm the formation of the dipole moment. Moreover, the change of the potential profile due to the heterostructure formation [green solid line in Fig. 5(d)] shows that potential drop happens mainly across the interface and extends to the 2L WS_2 layers. Such interfacial dipole moment can essentially be considered as an effective electric field (E-field), which is known to alter various properties of 2D layered materials. To understand such effect, we studied the electronic properties of a freestanding bilayer WS_2 structure under external E-field. The calculated atom-resolved projected band structure for the two WS_2 layers without and with E-field are summarized in Fig. 5(e), which shows that the coupled bilayer is electronically decoupled under E-field, behaving as two non-interacting monolayers. Interestingly, a clear indirect to direct transition is observed due to such E-field induced decoupling effect, which contributes to the enormous PL enhancement, consistent with the experimental observations.

Therefore, we attribute the PL enhancement observed experimentally to these two cooperative effect, i.e., p-doping effect that compensate the n-doping of the as exfoliated WS_2 and E-field induced electronic layer-layer decoupling. It is important to mention that similar charge transfer effect is also observed in heterostructures built by WS_2 and 2DPVSK with different thickness (Supporting information). The thicker the 2DPVSK the more charge transfer between the WS_2 and 2DPVSK, vice versa. Considering the E-field induced decoupling effect is only effective to multilayer systems and stronger charge transfer of the 2L WS_2/n=4 2DPVSK, the PL enhancement of the 2L WS_2/n=4 2DPVSK is expected to be stronger than that of the 1L WS_2/n=3 2DPVSK. This is indeed consistent with the 100 fold and 70 fold PL enhancement of the heterostructures 2L WS_2/n=4 2DPVSK and 1L WS_2/n=3 2DPVSK, respectively, compared to the WS_2. We note the interface curing strongly modify the system, leading to a much larger PL enhancement at a relatively lower energy. The enhancement in PL can be attributed to the reduction in defects, which increases the quantum efficiency of the emission. We anticipate that further theoretical and experimental study will reveal the atomic nature of interfacial structure and interactions between TMDCs and 2DPVSKs[30,33].

Conclusion

TMDCs and 2DPVSKs have emerged as highly promising materials for optoelectronic applications. However, TMDCs exhibit poor emission due to defect states and direct-to-indirect band transition, and 2DPVSKs suffer from poor stability towards ambient atmosphere. By combining these two materials in vertical heterostructures, we observed a significant enhancement of the photoemisison with respect to the bare TMDCs and 2DPVSKs, with relatively good stability. The PL enhancement is of the order of two orders of magnitude when we compare the heterostructures to the bare TMDCs. First-principle calculation shows that this PL enhancement can be attributed to charge transfer through the interface that generates dipole moment, which induces increased local effective electrical field, and such field results in in-direct to-

direct transition of electronic structure of 2L WS_2. Interestingly the PL emission amplitude and spectral distribution can be altered by interface curing in air under laser excitation, which induces further emission enhancement. The giant enhancement in the PL emission combined with largely improved stability under ambient condition and laser illumination may open opportunities for practical applications of the TMD/2DPVSK heterostructures in high efficiency optoelectronic devices.

AUTHOR INFORMATION

Corresponding Author

Corresponding Author: Aditya Mohite (adm4@rice.edu), Harry Atwater (haa@caltech.edu)

ACKNOWLEDGMENT

This work is part of the 'Photonics at Thermodynamic Limits' Energy Frontier Research Center funded by the U.S. Department of Energy, Office of Science, Office of Basic Energy Sciences under Award Number DE-SC0019140. We also acknowledge Northrop Grumman for financial support of instrumentation. A.Y and J.W acknowledges financial support from a Resnick Institute Fellowship. A.D.M and J.C.B acknowledge support by DOE-EERE DE-FOA-0001647 program. We acknowledge support from the Beckman Institute of the California Institute of Technology to the Molecular Materials Research Center. We are grateful to Prof. George R. Rossman for technical help, discussions, and support. We thank Prof. Jacky Even for useful discussions concerning the perovskite surface termination.

SUPPORTING INFORMATION

Additional information of experimental details, spatial variation of photoluminescence, measurement on 1L WS_2/n=3 2DPVSK samples, dielectric functions and photoluminescence excitation spectra, control experiments on WS_2/hBN and WS_2/BA samples, and details on first-principle calculations are outlined in Supporting Information.

REFERENCES

(1) Palacios-Berraquero, C.; Kara, D. M.; Montblanch, A. R.-P.; Barbone, M.; Latawiec, P.; Yoon, D.; Ott, A. K.; Loncar, M.; Ferrari, A. C.; Atatüre, M. Large-Scale Quantum-Emitter Arrays in Atomically Thin Semiconductors. *Nat. Commun.* **2017**, *8*, 15093.

(2) Gong, S.-H.; Alpeggiani, F.; Sciacca, B.; Garnett, E. C.; Kuipers, L. Nanoscale Chiral Valley-Photon Interface through Optical Spin-Orbit Coupling. *Science.* **2018**, *359* (6374), 443–447.

(3) Palacios-Berraquero, C.; Barbone, M.; Kara, D. M.; Chen, X.; Goykhman, I.; Yoon, D.; Ott, A. K.; Beitner, J.; Watanabe, K.; Taniguchi, T.; et al. Atomically Thin Quantum Light-Emitting Diodes. *Nat. Commun.* **2016**, *7*, 12978.

(4) Kang, D.-H.; Dugasani, S. R.; Park, H.-Y.; Shim, J.; Gnapareddy, B.; Jeon, J.; Lee, S.; Roh, Y.; Park, S. H.; Park, J.-H. Ultra-Low Doping on Two-Dimensional Transition Metal Dichalcogenides Using DNA Nanostructure Doped by a Combination of Lanthanide and Metal Ions. *Sci. Rep.* **2016**, *6*, 20333.

(5) Voiry, D.; Yang, J.; Chhowalla, M. Recent Strategies for Improving the Catalytic Activity of 2D TMD Nanosheets Toward the Hydrogen Evolution Reaction. *Adv. Mater.* **2016**, *28* (29), 6197–6206.

(6) Chen, M.; Xia, J.; Zhou, J.; Zeng, Q.; Li, K.; Fujisawa, K.; Fu, W.; Zhang, T.; Zhang, J.; Wang, Z.; et al. Ordered and Atomically Perfect Fragmentation of Layered Transition Metal Dichalcogenides via Mechanical Instabilities. *ACS Nano* **2017**, *11* (9), 9191–9199.

(7) Yuan, L.; Huang, L. Exciton Dynamics and Annihilation in WS2 2D Semiconductors. *Nanoscale* **2015**, *7*, 7402–7408.

(8) Zhao, W.; Ghorannevis, Z.; Chu, L.; Toh, M.; Kloc, C.; Tan, P.-H.; Eda, G. Evolution of Electronic Structure in Atomically Thin Sheets of WS2 AndWSe2. *ACS Nano* **2013**, *7* (1), 791–797.

(9) Cao, D. H.; Stoumpos, C. C.; Farha, O. K.; Hupp, J. T.; Kanatzidis, M. G. 2D Homologous Perovskites as Light-Absorbing Materials for Solar Cell Applications. *J. Am. Chem. Soc.* **2015**, *137* (24), 7843–7850.

(10) Tsai, H.; Nie, W.; Blancon, J.-C.; Stoumpos, C. C.; Asadpour, R.; Harutyunyan, B.; Neukirch, A. J.; Verduzco, R.; Crochet, J. J.; Tretiak, S.; et al. High-Efficiency Two-Dimensional Ruddlesden–Popper Perovskite Solar Cells. *Nature* **2016**, *536* (7616), 312–316.

(11) Xing, J.; Zhao, Y.; Askerka, M.; Quan, L. N.; Gong, X.; Zhao, W.; Zhao, J.; Tan, H.; Long, G.; Gao, L.; et al. Color-Stable Highly Luminescent Sky-Blue Perovskite Light-Emitting Diodes. *Nat. Commun.* **2018**, *9* (1), 1–8.

(12) Yuan, M.; Quan, L. N.; Comin, R.; Walters, G.; Sabatini, R.; Voznyy, O.; Hoogland, S.; Zhao, Y.; Beauregard, E. M.; Kanjanaboos, P.; et al. Perovskite Energy Funnels for Efficient Light-Emitting Diodes. *Nat. Nanotechnol.* **2016**, *11* (10), 1–27.

(13) Lin, K.; Xing, J.; Quan, L. N.; de Arquer, F. P. G.; Gong, X.; Lu, J.; Xie, L.; Zhao, W.; Zhang, D.; Yan, C.; et al. Perovskite Light-Emitting Diodes with External Quantum Efficiency Exceeding 20 per Cent. *Nature* **2018**, *562* (7726), 245–248.

(14) Yan, F.; Xing, J.; Xing, G.; Quan, L.; Tan, S. T.; Zhao, J.; Su, R.; Zhang, L.; Chen, S.; Zhao, Y.; et al. Highly Efficient Visible Colloidal Lead-Halide Perovskite Nanocrystal Light-Emitting Diodes. *Nano Lett.* **2018**, *18* (5), 3157–3164.

(15) Tsai, H.; Nie, W.; Blancon, J.-C.; Stoumpos, C. C.; Soe, C. M. M.; Yoo, J.; Crochet, J.; Tretiak, S.; Even, J.; Sadhanala, A.; et al. Stable Light-Emitting Diodes Using Phase-Pure Ruddlesden--Popper Layered Perovskites. *Adv. Mater.* **2018**, *30* (6), 1704217.

(16) Gong, X.; Voznyy, O.; Jain, A.; Liu, W.; Sabatini, R.; Piontkowski, Z.; Walters, G.; Bappi, G.; Nokhrin, S.; Bushuyev, O.; et al. Electron--Phonon Interaction in Efficient Perovskite Blue Emitters. *Nat. Mater.* **2018**, *17* (6), 550.

(17) Blancon, J.-C.; Tsai, H.; Nie, W.; Stoumpos, C. C.; Pedesseau, L.; Katan, C.; Kepenekian, M.; Soe, C. M. M.; Appavoo, K.; Sfeir, M. Y.; et al. Extremely Efficient Internal Exciton Dissociation through Edge States in Layered 2D Perovskites. *Science.* **2017**, No. March, 1–10.

(18) Fang, H. H.; Yang, J.; Tao, S.; Adjokatse, S.; Kamminga, M. E.; Ye, J.; Blake, G. R.; Even, J.; Loi, M. A. Unravelling Light-Induced Degradation of Layered Perovskite Crystals and Design of Efficient Encapsulation for Improved Photostability. *Adv. Funct. Mater.* **2018**, *28* (21).

(19) Wang, H.; Liu, F.; Fu, W.; Fang, Z.; Zhou, W.; Liu, Z. Two-Dimensional Heterostructures: Fabrication, Characterization, and Application. *Nanoscale* **2014**, *6* (21), 12250–12272.

(20) Pomerantseva, E.; Gogotsi, Y. Two-Dimensional Heterostructures for Energy Storage. *Nat. Energy* **2017**, *2* (7), 17089.

(21) Ishihara, T.; Takahashi, J.; Goto, T. Optical Properties Due to Electronic Transitions in Two-Dimensional Semiconductors (C,,H2n+1NH3)PbI4. *Phys. Rev. B* **1990**, *42* (17), 99–107.

(22) Mak, K. F.; He, K.; Shan, J.; Heinz, T. F. Control of Valley Polarization in Monolayer MoS2by Optical Helicity. *Nat. Nanotechnol.* **2012**, *7* (8), 494–498.

(23) Blancon, J. C.; Stier, A. V.; Tsai, H.; Nie, W.; Stoumpos, C. C.; Traoré, B.; Pedesseau, L.; Kepenekian, M.; Katsutani, F.; Noe, G. T.; et al. Scaling Law for Excitons in 2D Perovskite Quantum Wells. *Nat. Commun.* **2018**, *9* (1), 1–10.

(24) Wang, G.; Chernikov, A.; Glazov, M. M.; Heinz, T. F.; Marie, X.; Amand, T.; Urbaszek, B. Colloquium: Excitons in Atomically Thin Transition Metal Dichalcogenides. *Rev. Mod. Phys.* **2018**, *90* (2), 21001.

(25) Even, J.; Pedesseau, L.; Katan, C. Understanding Quantum Confinement of Charge Carriers in Layered 2D Hybrid Perovskites. *ChemPhysChem* **2014**, *15* (17), 3733–3741.

(26) Peimyoo, N.; Yang, W.; Shang, J.; Shen, X.; Wang, Y.; Yu, T. Chemically Driven Tunable Light Emission of Charged and Neutral Excitons in Monolayer WS2. *ACS Nano* **2014**, *8* (11), 11320–11329.

(27) Chakraborty, B.; Bera, A.; Muthu, D. V. S.; Bhowmick, S.; Waghmare, U. V.; Sood, A. K. Symmetry-Dependent Phonon

Renormalization in Monolayer MoS2 Transistor. *Phys. Rev. B - Condens. Matter Mater. Phys.* **2012**, *85* (16), 2–5.

(28) Wurstbauer, U.; Miller, B.; Parzinger, E.; Lin, Z.; Carvalho, B. R.; Kahn, E.; Brien, M. O.; Mcevoy, N.; Motta, C.; Wang, F.; et al. Strain-Induced Phonon Shifts in Tungsten Disul Fi de Nanoplatelets and Nanotubes. *2D Mater.* **2016**, *4*, 015007.

(29) He, Z.; Xu, W.; Zhou, Y.; Wang, X.; Sheng, Y.; Rong, Y.; Guo, S.; Zhang, J.; Smith, J. M.; Warner, J. H. Biexciton Formation in Bilayer Tungsten Disulfide. *ACS Nano* **2016**, *10* (2), 2176–2183.

(30) Volonakis, G.; Giustino, F. Interfaces Between Graphene-Related Materials and MAPbI3: Insights from First-Principles. *Adv. Mater. Interfaces* **2018**, *5* (22), 1800496.

(31) Mao, L.; Ke, W.; Pedesseau, L.; Wu, Y.; Katan, C.; Even, J.; Wasielewski, M. R.; Stoumpos, C. C.; Kanatzidis, M. G. Hybrid Dion--Jacobson 2D Lead Iodide Perovskites. *J. Am. Chem. Soc.* **2018**, *140* (10), 3775–3783.

(32) Myae, C.; Soe, M.; Stoumpos, C. C.; Kepenekian, M. M.; Traore, B.; Tsai, H.; Nie, W.; Wang, B.; Katan, C.; Seshadri, R.; et al. New Type of 2D Perovskites with Alternating Cations in the Interlayer Space,(C (NH2) 3)(CH3NH3) n Pb n I3 N+ 1: Structure, Properties, and Photovoltaic Performance. *J. Am. Chem. Soc.* **2017**, *139* (45), 16297–16309.

(33) Nie, W.; Tsai, H.; Blancon, J.-C.; Liu, F.; Stoumpos, C. C.; Traore, B.; Kepenekian, M.; Durand, O.; Katan, C.; Tretiak, S.; et al. Critical Role of Interface and Crystallinity on the Performance and Photostability of Perovskite Solar Cell on Nickel Oxide. *Adv. Mater.* **2018**, *30* (5), 1703879.

(34) Ferreira, A. C.; Létoublon, A.; Paofai, S.; Raymond, S.; Ecolivet, C.; Rufflé, B.; Cordier, S.; Katan, C.; Saidaminov, M. I.; Zhumekenov, A. A.; et al. Elastic Softness of Hybrid Lead Halide Perovskites. *Phys. Rev. Lett.* **2018**, *121* (8), 1–6.

(35) Kepenekian, M.; Traore, B.; Blancon, J. C.; Pedesseau, L.; Tsai, H.; Nie, W.; Stoumpos, C. C.; Kanatzidis, M. G.; Even, J.; Mohite, A. D.; et al. Concept of Lattice Mismatch and Emergence of Surface States in Two-Dimensional Hybrid Perovskite Quantum Wells. *Nano Lett.* **2018**, *18* (9), 5603–5609.

(36) Fan, Z.; Xiao, H.; Wang, Y.; Zhao, Z.; Lin, Z.; Cheng, H. C.; Lee, S. J.; Wang, G.; Feng, Z.; Goddard, W. A.; et al. Layer-by-Layer Degradation of Methylammonium Lead Tri-Iodide Perovskite Microplates. *Joule* **2017**, *1* (3), 548–562.

(37) He, Z.; Wang, X.; Xu, W.; Zhou, Y.; Sheng, Y.; Rong, Y.; Smith, J. M.; Warner, J. H. Revealing Defect-State Photoluminescence in Monolayer WS2 by Cryogenic Laser Processing. *ACS Nano* **2016**, *10* (6), 5847–5855.

(38) Zhao, W.; Ribeiro, R. M.; Toh, M.; Carvalho, A.; Kloc, C.; Neto, A. H. C.; Eda, G. Origin of Indirect Optical Transitions in Few-Layer MoS 2 , WS 2 , and WSe 2. *Nano Lett.* **2013**, *13*, 5627–5634.

(39) Molas, M. R.; Nogajewski, K.; Slobodeniuk, A. O.; Binder, J.; Bartos, M.; Potemski, M. Optical Response of Monolayer, Few-Layer and Bulk Tungsten Disulfide. *Nanoscale* **2017**, *9*, 13128–13141.

(40) Keyshar, K.; Berg, M.; Zhang, X.; Vajtai, R.; Gupta, G.; Chan, C. K.; Beechem, T. E.; Ajayan, P. M.; Mohite, A. D.; Ohta, T. Experimental Determination of the Ionization Energies of $MoSe_2$, WS_2, and MoS_2 on SiO_2 Using Photoemission Electron Microscopy. *ACS Nano* **2017**, acsnano.7b03242.

(41) Guo, P.; Huang, W.; Stoumpos, C. C.; Mao, L.; Gong, J.; Zeng, L.; Diroll, B. T.; Xia, Y.; Ma, X.; Gosztola, D. J.; et al. Hyperbolic Dispersion Arising from Anisotropic Excitons in Two-Dimensional Perovskites. *Phys. Rev. Lett.* **2018**, *121* (12), 127401.

(42) Li, Y.; Chernikov, A.; Zhang, X.; Rigosi, A.; Hill, H. M.; Van Der Zande, A. M.; Chenet, D. A.; Shih, E. M.; Hone, J.; Heinz, T. F. Measurement of the Optical Dielectric Function of Monolayer Transition-Metal Dichalcogenides: MoS2, Mo S E2, WS2, and WSe2. *Phys. Rev. B - Condens. Matter Mater. Phys.* **2014**, *90* (20), 1–6.

(43) Kozawa, D.; Carvalho, A.; Verzhbitskiy, I.; Giustiniano, F.; Miyauchi, Y.; Mouri, S.; Castro Neto, A. H.; Matsuda, K.; Eda, G. Evidence for Fast Interlayer Energy Transfer in MoSe2/WS2 Heterostructures. *Nano Lett.* **2016**, *16* (7), 4087–4093.

(44) Su, H.; Deng, A.; Zhen, Z.; Dai, J. F. Γ-Valley Assisted Intervalley Scattering in Monolayer and Bilayer WS2 Revealed by Time-Resolved Kerr Rotation Spectroscopy. *Phys. Rev. B* **2018**, *97* (11), 1–8.